coatings

MDPI

Article

Experimental Study on the Optimal Mix Proportion of Steel Fiber-Reinforced Concrete in Cold Regions

Li-Ming Wu [1,2], Feng Gao [1], Guang-Na Liu [2,*], Hu-Xin-Tong Huang [3,*], Zi-Jian Wang [3], Yue Wang [2] and Wen-Jie Luo [3]

[1] School of Civil Engineering, Chongqing Jiaotong University, Chongqing 400074, China
[2] School of Urban Construction Engineering, Chongqing Technology and Business Institute, Chongqing 400052, China
[3] School of Civil and Hydraulic Engineering, Chongqing University of Science & Technology, Chongqing 401331, China
* Correspondence: liugl@cqtbi.edu.cn (G.-N.L.); 2024206056@cqust.edu.cn (H.-X.-T.H.)

Abstract

To determine the optimal mix proportion of steel fiber-reinforced concrete in cold regions, this study adopted a multi-factor orthogonal experimental design method. A series of mix proportion schemes was formulated based on different water-to-binder ratios, steel fiber volume fractions, and combinations of mineral admixtures such as silica fume. Mechanical performance tests and freeze–thaw cycle tests were conducted to obtain the strength, deformation characteristics, and durability degradation patterns of specimens with different mix proportions before and after freeze–thaw exposure. Meanwhile, scanning electron microscopy (SEM) was employed to observe the microscopic surface morphology of specimens, both pre- and post-freeze–thaw cycles, and to analyze the damage evolution in pore structures and the fiber–matrix interfacial transition zone, thereby elucidating the microscopic mechanism of freeze–thaw damage. Ultimately, by comprehensively comparing the macro-mechanical properties, freeze–thaw durability, and microstructural characteristics, the experimental results of different groups were evaluated to identify the optimal mix proportion for steel fiber-reinforced concrete, which exhibits excellent mechanical performance and durability under freeze–thaw conditions. The results indicated that freeze–thaw cycles significantly reduced the mechanical properties of the concrete. The optimal mix proportion was achieved with a water-to-binder ratio of 0.4, a silica fume content of 10%, and a steel fiber volume fraction of 1.5%. This optimal mix proportion can provide a direct reference for the material design and application of steel fiber-reinforced concrete in engineering projects located in cold regions.

Keywords: tunnel lining; steel fiber-reinforced concrete; orthogonal experiment; freeze–thaw cycle; scanning electron microscopy (SEM)

Check for updates

Academic Editor: Edoardo Proverbio

Received: 31 January 2026
Revised: 18 February 2026
Accepted: 20 February 2026
Published: 23 February 2026

Copyright: © 2026 by the authors. Licensee MDPI, Basel, Switzerland. This article is an open access article distributed under the terms and conditions of the Creative Commons Attribution (CC BY) license.

1. Introduction

In high-altitude and extremely cold regions, freeze–thaw damage to concrete is one of the critical issues affecting structural durability and safety. Studies have shown that freeze–thaw cycles significantly accelerate the performance degradation of concrete, threatening the long-term service life of engineering structures. As the primary building material, the mechanical properties of concrete directly influence structural design, construction quality, and long-term safety. Therefore, investigating the mechanical behavior of steel fiber-reinforced concrete under freeze–thaw conditions is of great significance for optimizing

material mix design, enhancing frost resistance, and extending service life. However, existing research on steel fiber-reinforced concrete under combined freeze–thaw and loading conditions remains insufficient, particularly in terms of characterizing interfacial damage evolution and cumulative performance degradation processes.

Lin et al. [1] conducted freeze–thaw experiments on steel fiber-reinforced concrete (SFRC) with different strength grades, analyzing the effects of strength grade and number of freeze–thaw cycles on compressive strength, mass loss, and microstructure. They established a damage model based on RDEM (Relative Dynamic Modulus of Elasticity). The results indicated that low-strength SFRC exhibited significant damage, with a maximum strength loss of up to 35.02% after 125 freeze–thaw cycles. In contrast, high-strength SFRC maintained better performance and a denser microstructure. Sun et al. [2] investigated the impact of freeze–thaw cycles and steel fiber content on the dynamic mechanical properties of SFRC using a Split Hopkinson Pressure Bar (SHPB) apparatus. The results showed that as the number of freeze–thaw cycles increased, the dynamic compressive strength decreased while the peak strain increased. With higher fiber content, the dynamic compressive strength initially increased and then decreased, whereas the peak strain generally increased. The study recommended an optimal fiber content of 2%. Ding et al. [3] explored the influence of silica fume content on the compressive strength and mass loss of concrete under coupled wet–dry and freeze–thaw conditions. They found that increasing silica fume content effectively reduced the total porosity and average pore diameter, decreased the number of harmful pores larger than 100 nm, and increased the fractal dimension of pores. This reflected an enhancement in pore structure complexity and compactness. Xuan et al. [4] conducted pull-out and microhardness tests, demonstrating that the addition of silica fume can effectively enhance the interfacial bond strength, reduce the thickness of the near-surface weak zone, and improve the microstructure of the interfacial transition zone (ITZ). Zhang et al. [5] investigated the influence of silica fume content on the frost resistance and mechanical properties of concrete based on the rapid freezing method, ultimately concluding that incorporating silica fume can effectively improve the frost resistance of concrete. Zhou et al. [6] studied the effects of freeze–thaw cycles and steel fiber content on the dynamic mechanical properties of concrete through experiments and SEM analysis. The results showed that freeze–thaw cycles lead to a reduction in axial compressive strength and an increase in peak strain; a 1% steel fiber content can significantly improve the dynamic performance and energy absorption capacity of concrete after freeze–thaw deterioration. Bai et al. [7] investigated the influence of different steel fiber contents on the mechanical properties and microscopic morphology of concrete, concluding that steel fibers have a limited effect on improving the compressive strength of concrete but can significantly enhance its splitting tensile and flexural strengths. At a content of 1.5%, the splitting tensile strength increased by 80%, and the macroscopic properties were consistent with the microstructure characteristics. Dong [8] studied the effects of freeze–thaw cycles on the mechanical properties of hybrid steel–polypropylene fiber-reinforced concrete. The results indicated that the strength of FRC remained stable after 250 freeze–thaw cycles, but its deformation capacity significantly decreased. Microscopic single-fiber pull-out tests revealed that freeze–thaw action primarily damages the fiber–matrix interfacial bond, which is the main cause of the deterioration in FRC ductility. Zheng et al. [9] investigated the influence of freeze–thaw cycles on the thermophysical and mechanical properties of concrete, analyzed the mechanisms of multiple factors such as water–binder ratio and air content, summarized the evolution of microstructure, damage theories, and assessment methods, and provided suggestions for future research on multiscale modeling and damage mechanisms under complex environmental conditions.

Current research predominantly focuses on the material properties and damage monitoring of steel fiber-reinforced concrete under normal temperature conditions, while studies on its applicability in high-altitude cold regions remain insufficient. In particular, there is a lack of systematic analysis on the coupling mechanism between material performance degradation and structural damage under long-term freeze–thaw cycles. Based on the characteristics of the actual freeze–thaw environment, the number of freeze–thaw cycles was set to 100. Regarding fiber reinforcement, existing research has primarily focused on the single incorporation of steel fibers or the hybrid incorporation of steel fibers with other fibers. However, this study emphasizes the synergistic effect of steel fibers (0%, 1%, 1.5%) and silica fume (0%, 5%, 10%) on the macroscopic and microscopic damage mechanisms of concrete under freeze–thaw cycles. To further clarify the contribution of steel fibers to material performance, the water-to-binder ratio was fixed at 0.4 to eliminate its potential interference with the test results. Therefore, it is imperative to investigate the mechanical properties and failure mechanisms of steel fiber-reinforced concrete under freeze–thaw conditions, in order to elucidate the deterioration mechanisms at the fiber–matrix interface under the coupled effects of long-term freeze–thaw cycles and loading. This will provide a theoretical basis for material optimization in extreme environments.

2. Mix Design and Test Methods

The mechanical properties of steel fiber-reinforced concrete are significantly influenced by the mix proportion of raw materials and the dosage of admixtures, necessitating the selection of an optimal mix through appropriate experimental methods. Orthogonal experimental design, which enables systematic analysis of multi-factor influences with a relatively small number of specimens, has been established as an effective approach for optimizing mix proportions. This method allows for the identification of the contribution of each component to concrete performance through representative combinations of conditions, thereby providing a basis for material optimization [10]. Building on preliminary preparations, an orthogonal experiment was conducted considering factors such as freeze–thaw cycles, steel fiber content, and silica fume content. Specimens were prepared, and their mechanical properties were tested, with the aim of identifying the mix proportion that exhibits optimal frost resistance. The findings are expected to provide a scientific reference for the modification of concrete used in tunnel linings in cold regions.

2.1. Mix Design

Based on existing research findings [11], the designed concrete strength for the experiments was selected as C40, with a water–cement ratio set at 0.4. Plain concrete and steel fiber-reinforced concrete served as the primary subjects of investigation. Specimens of both concrete types were first prepared, followed by laboratory mechanical performance tests to obtain their compressive, splitting tensile, and flexural strengths, as well as elastic modulus under freeze–thaw cycles. Mass loss rate and strength loss rate were monitored simultaneously. By integrating scanning electron microscopy (SEM) to observe microstructural interface damage characteristics and applying response surface methodology to quantify the influence weights of various factors on the deterioration, the evolution of mechanical properties of steel fiber-reinforced concrete with the number of freeze–thaw cycles was clarified. This approach further reveals the interface enhancement mechanism by which steel fibers inhibit freeze–thaw damage in concrete. The corresponding detailed mix proportions are presented in Tables 1 and 2.

Table 1. Mix proportion design scheme for specimens.

No.	Silica Fume Content (A)	Steel Fiber Volume Fraction (B)	Water-to-Binder Ratio	Water Reducer
S	0	0	0.40	1%
SF1	5%	1%	0.40	1%
SF2	10%	1%	0.40	1%
SF3	5%	1.5%	0.40	1%
SF4	10%	1.5%	0.40	1%

Table 2. Design parameters for specimens (Unit: g).

No.	Water	Cement	Silica Fume	Coarse Aggregate	Sand	Steel Fiber Volume Fraction
S	195	445	0	867.3	907.7	0
SF1	195	425	20	812.7	907.7	54.6
SF2	195	405	40	812.7	907.7	54.6
SF3	195	425	20	785.4	907.7	81.9
SF4	195	405	40	785.4	907.7	81.9

2.2. Test Materials

2.2.1. Cement

As a key matrix material in steel fiber-reinforced concrete, the performance indicators of cement directly influence the workability and mechanical properties of the concrete. In accordance with the specifications outlined in the "Common Portland Cement GB175-2007" standard [12], the cement used in this study is P.O42.5 ordinary Portland cement produced by Anhui Xuancheng Conch Cement Co., Ltd. (Xuancheng, China) under the Conch brand. The relevant performance parameters of this cement are tested and presented in Table 3.

Table 3. Main parameters of the test cement.

Main Parameters	Density/(g/cm^3)	Initial Setting Time/min	Final Setting Time/min	Specific Surface Area/(m^2/kg)	Loss on Ignition/%
Strength grade 42.5 cement	3.07	233	293	355	3.2

2.2.2. Silica Fume

According to reference studies [13], silica fume can significantly enhance the workability and mechanical properties of concrete. It reacts with cement hydration products to form additional cementitious compounds, effectively filling the micro-voids between concrete particles, thereby improving concrete compactness. This process leads to enhanced mechanical performance and durability. Additionally, silica fume helps control the shrinkage and cracking tendencies of concrete, contributing to higher strength and improved long-term durability. In compliance with the requirements of "Silica Fume for Mortar and Concrete GB/T 27690-2023" [14], Borun-brand silica fume was used in this study. The silica fume is shown in Figure 1, and its key parameters are listed in Table 4.

Table 4. Main physical parameters of silica fume.

Main Parameters	Density/(g/cm^3)	Average Particle Size/μm	Specific Surface Area/(m^2/g)	Color	Loss on Ignition/%
Index	2.2	0.3	21.2	Off-white	3.92

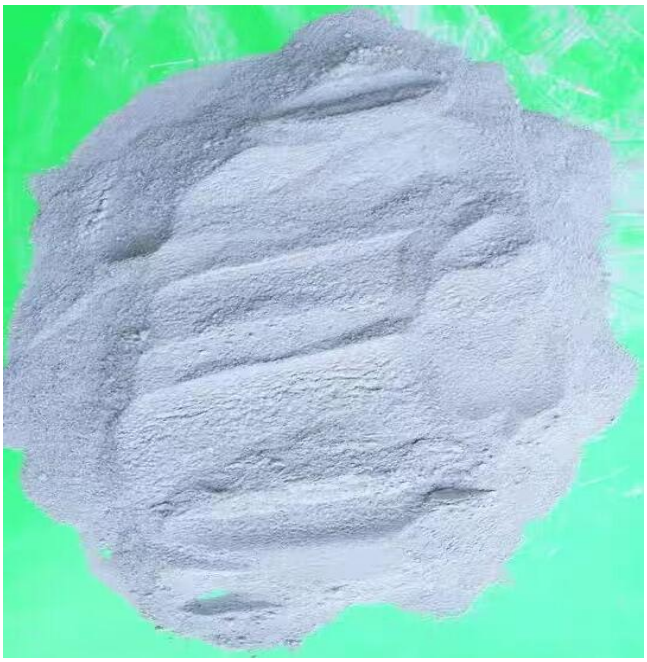

Figure 1. Silica fume.

2.2.3. Aggregates

For this experiment, the coarse aggregate consisted of crushed stone that met the requirements of continuous gradation, with a maximum particle size not exceeding 20 mm or two-thirds of the steel fiber length. The selected coarse and fine aggregates complied with the "Test Methods of Aggregate for Highway Engineering JTG 3432-2024" [15], as illustrated in Figure 2. The fine aggregate was natural river sand sourced from Chongqing. According to the "Sand for Construction GB14684-2022" [16], its fineness modulus was determined to be 2.6, as shown in Figure 3. The sieve analysis results are presented in Table 5.



Figure 2. Crushed stone.



Figure 3. Sand.

Table 5. Sieving test results of coarse aggregates.

Sieve Mesh Size (mm)		2.36	4.75	9.5	16	19	26.5
Cumulative percentage retained for 4.75–19 mm (%)	Upper limit	100	95	75	45	5	0
	Lower limit	95	85	60	30	0	0
	Median value	97.5	90	67.5	37.5	2.5	0
	Measured value	100	90	68	33	3	0

2.2.4. Water Reducer

The experiment employed a polycarboxylate-based high-performance water reducer, whose primary functions include improving the workability of concrete, reducing the mixing water requirement, effectively inhibiting concrete shrinkage, and enhancing the durability of concrete. In accordance with the specifications outlined in the "Concrete Admixtures GB8076-2023" standard [17], the key performance indicators of the water reducer used in this study are presented in Table 6.

Table 6. Main performance indicators of water-reducing agent.

Name	PH Value	Air Content/%	Bleeding Rate/%	Water Reduction Rate/%	Solid Content/%
HLX	6.1	3	20	27	38.2

2.2.5. Steel Fibers

Currently, a wide variety of steel fiber types are available both domestically and internationally. Considering cost-effectiveness and comprehensive performance indicators, milled wave-shaped steel fibers were selected for this study. In accordance with the standard "Fibers for Cement Concrete in Highway Engineering JT/T 524-2019" [18], the key performance parameters of the steel fibers used are detailed in Table 7.

Table 7. Milling-type steel fibers.

Fiber Name	Tensile Strength (MPa)	Equivalent Diameter (mm)	Fiber Length (mm)
Milling type	fu = 650	2.4 ± 1	32 ± 3

2.3. Test Methods

2.3.1. Preparation of Concrete Specimens

Specimens with dimensions of 100 mm × 100 mm × 400 mm and 100 mm × 100 mm × 100 mm were cast for the experiments, as detailed in Table 8.

Table 8. Mechanical performance test groups of concrete specimens.

Test Indicator	Specimen Dimensions	Number of Specimen Groups	Number Per Group (Pieces)
Compressive strength test	100 mm × 100 mm × 100 mm	5	3
Splitting tensile strength test	100 mm × 100 mm × 100 mm	5	3
Flexural strength test	100 mm × 100 mm × 400 mm	5	3

A 100 L forced-action mixer and a table vibrator were used for mixing and compaction. The procedure was as follows: sand, coarse aggregate, silica fume, and cement were first dry-mixed. Steel fibers were then added in three separate batches and mixed with the dry materials. Finally, water and superplasticizer were added, and mixing continued until the steel fibers were uniformly dispersed [19]. After placing the concrete into molds, the surface was covered with plastic film to prevent moisture evaporation from the specimen surfaces. The molds were removed after 24 h, and the specimens were subsequently cured under standard conditions for 28 days, as shown in Figures 4 and 5.



Figure 4. Curing of specimens before demolding.



Figure 5. Concrete curing chamber.

2.3.2. Freeze–Thaw Cycle Tests

The tests were conducted in accordance with the "Standard for Test Methods of Long-term Performance and Durability of Concrete (GB/T50082-2024)" [20] and the "Steel Fibers for Concrete (GB/T 39147-2020)" [21]. After standard curing, the specimens were removed, and those designated for freeze–thaw cycling were immersed in water at (20 ± 2) °C for 4 days, as shown in Figure 6. For temperature-monitoring specimens, temperature sensors were embedded at their centers, with antifreeze solution used as the freeze–thaw medium. For the main test specimens, clean water was employed as the freeze–thaw medium. The freeze–thaw tests were performed using a high-low temperature humidity test chamber (BHT5008F), as illustrated in Figure 7. The freezing temperature for the test specimens ranged from −18 °C to −14 °C, while the thawing temperature ranged from 5 °C to 8 °C. Each freeze–thaw cycle lasted between 2 and 4 h.



Figure 6. Water immersion of specimens.



Figure 7. High-low temperature humidity test chamber.

2.3.3. Performance Tests

The fundamental mechanical properties of concrete serve as its most critical indicators, providing the essential basis for determining its strength grade and representing primary factors that govern other significant performance characteristics and parameters [22]. In order to gain deeper insights into the influence of freeze–thaw cycles on the frost damage mechanisms and fundamental mechanical properties of steel fiber-reinforced concrete, this study investigates freeze–thaw cycles at 25, 50, 75, and 100 cycles. The temperature gradient settings for one freeze–thaw cycle are illustrated in Figure 8.

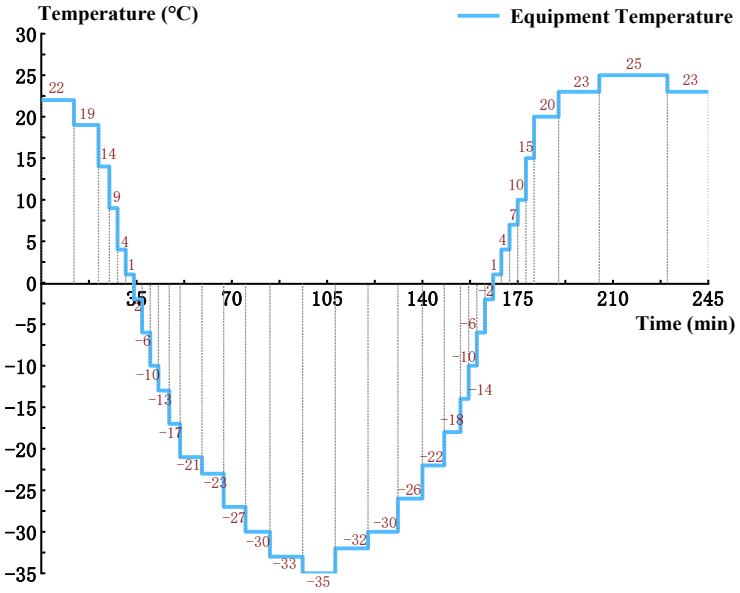

Figure 8. Temperature gradient during one cycle of freeze–thaw testing.

Seventy-five specimens each for flexural, compressive, and splitting tensile tests were subjected to freeze–thaw cycling experiments, with the specimens illustrated in Figures 9 and 10. Physical parameters of the steel fiber-reinforced concrete (SFRC) specimens under freeze–thaw cycles, including mass, elastic modulus, compressive strength, and flexural strength, were measured. The equipment utilized primarily consisted of a dynamic modulus tester, mass balance, universal testing machine, and compression testing machine. The experimental setup and apparatus employed are shown in Figure 11.



Figure 9. Prism specimen.



Figure 10. Cube specimen.



(**a**) DT-20 Dynamic Modulus Tester

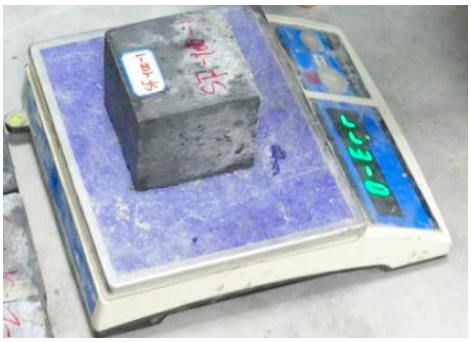

(**b**) Concrete Weighing

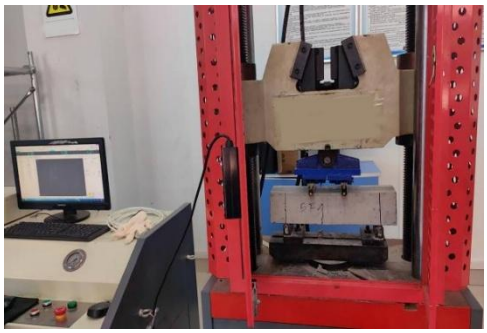

(**c**) WAW-300 Universal Testing Machine (Flexural Test)

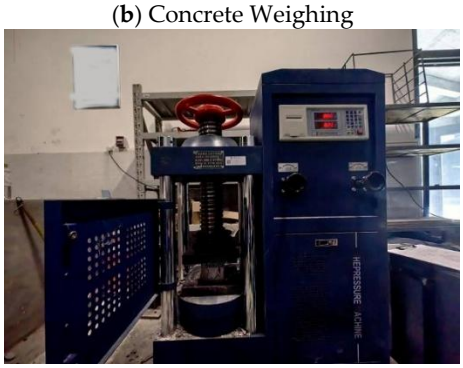

(**d**) DYE-200B Compression Testing Machine (Compressive Test)



(**e**) WAW-300 Universal Testing Machine (Splitting Test)



(**f**) Freeze–Thaw Cycling Test Chamber

Figure 11. Test equipment.

3. Test Observations

3.1. Surface Morphology of Specimens After Freeze–Thaw Cycles

Figures 12 and 13 illustrate the apparent changes of three groups of prismatic steel fiber-reinforced concrete specimens subjected to 0~100 freeze–thaw cycles. Upon observation after 25 freeze–thaw cycles, localized concrete spalling was noted at the edges of the specimens in all five groups, accompanied by noticeable surface sanding, while no exposed steel fibers were observed in the steel fiber-reinforced concrete. After 50 freeze–thaw cycles, the surface layer of the concrete specimens began to detach extensively, partially revealing fibers and distinctly exposing coarse aggregates, with the appearance of pitted and honeycombed pores. By 75 freeze–thaw cycles, surface concrete spalling became pronounced, aggregate exposure increased, localized steel fiber exposure became more frequent, and the extent of surface pitting expanded. After 75 freeze–thaw cycles, the concrete specimens exhibited significant apparent spalling, more evident aggregate exposure, severe exposure of steel fibers in the steel fiber-reinforced concrete specimens, and a considerable amount of concrete debris.

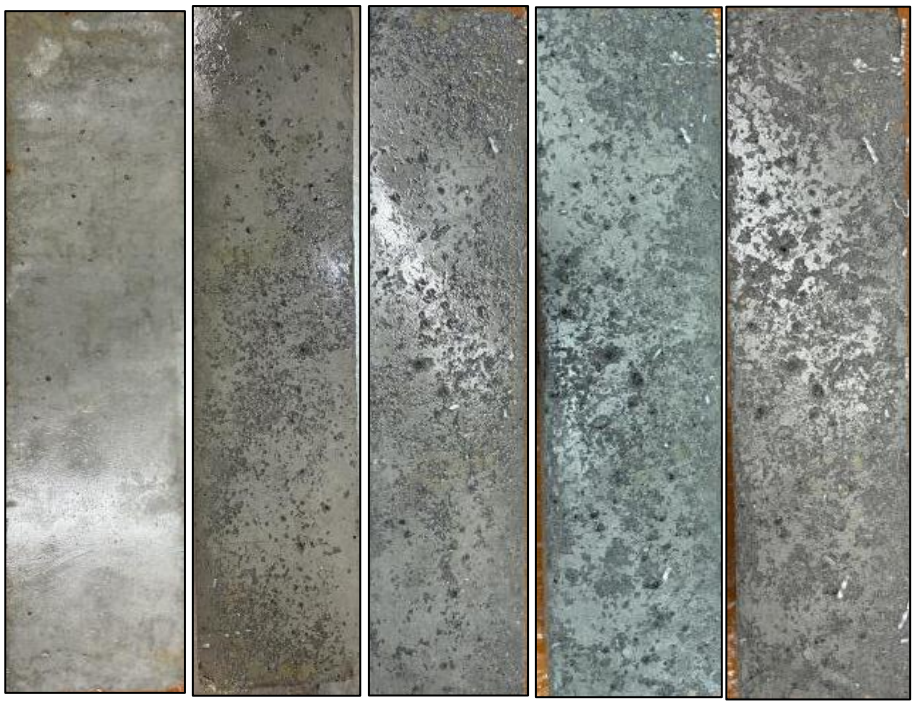

(**a**) 0 freeze–thaw cycles (**b**) 25 freeze–thaw cycles (**c**) 50 freeze–thaw cycles (**d**) 75 freeze–thaw cycles (**e**) 100 freeze–thaw cycles

Figure 12. Apparent phenomena of SF prism specimens after freeze–thaw cycles.

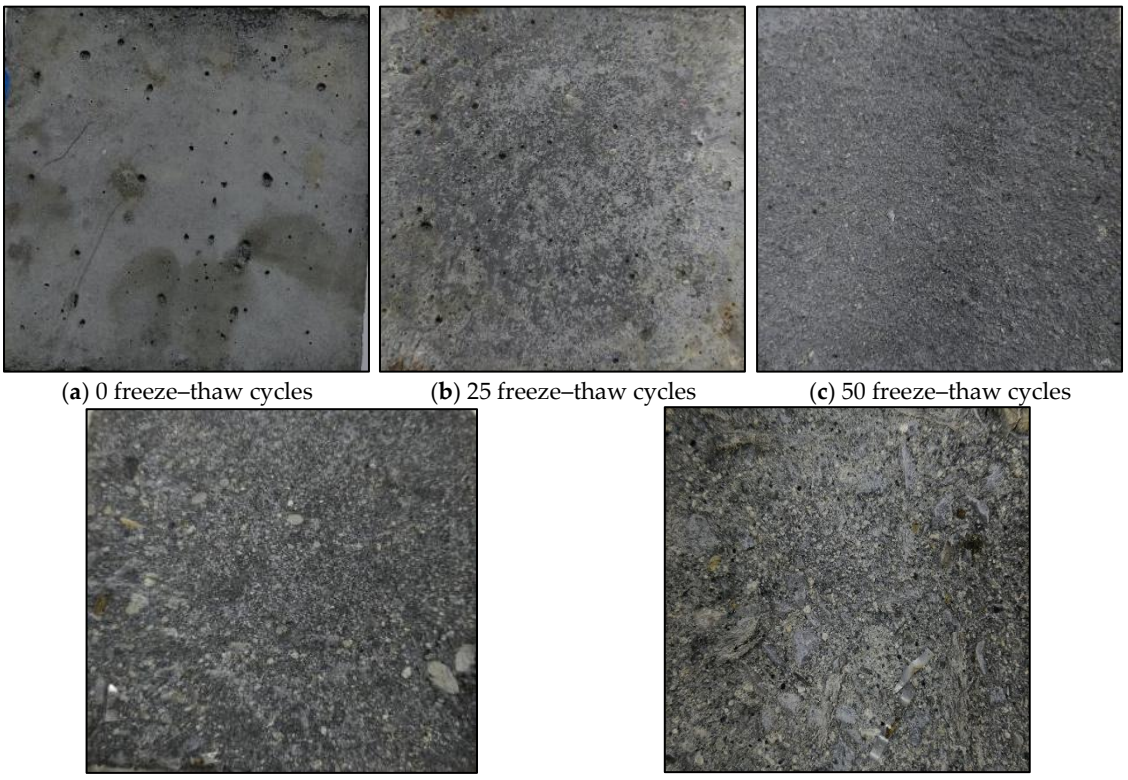

(**a**) 0 freeze–thaw cycles (**b**) 25 freeze–thaw cycles (**c**) 50 freeze–thaw cycles

(**d**) 75 freeze–thaw cycles (**e**) 100 freeze–thaw cycles

Figure 13. Apparent phenomena of SF cubic specimens after freeze–thaw cycles.

3.2. Failure Modes of Specimens

3.2.1. Compression Tests

After curing, freeze–thaw cycling, and mass testing for each specimen group, compressive tests were conducted on all groups using a DYE-2000B compression testing machine. The process of compressive testing and the resulting failure specimens are illustrated in Figure 14.



(**a**) Compression test (**b**) Specimen after compression failure

Figure 14. Compression test of the specimen.

With the increase in freeze–thaw cycles, the failure mode gradually transitions to spalling failure. This is primarily attributed to the weakening of the interfacial transition zone between the cement matrix and the aggregates or fibers caused by freeze–thaw damage. The observed phenomenon was compared with existing studies, which also reported interfacial debonding after multiple freeze–thaw cycles, and this is considered the main reason for the sudden drop in load-bearing capacity. Furthermore, it was found that after 100 freeze–thaw cycles, the steel fibers enabled the specimen to maintain a certain level of integrity, reflecting the bridging effect of the fibers.

3.2.2. Flexural Tests

Following the curing, freeze–thaw cycling tests, and mass measurements of each specimen group, flexural tests were conducted on all groups using a WAW-300 universal testing machine. The compressive testing process and the specimens after flexural failure are illustrated in Figure 15.



(**a**) Flexural test (**b**) Specimen after flexural failure

Figure 15. Flexural test of the specimen.

With the increase in the number of freeze–thaw cycles, freeze–thaw action has a significant impact on both fracture toughness and crack propagation. Consistent with previous studies, steel fiber-reinforced concrete exhibits a loss of toughness after freeze–thaw cycles, which leads to a decrease in flexural strength as the number of freeze–thaw cycles increases.

3.2.3. Splitting Tests

Following the curing, freeze–thaw cycling tests, and mass measurements of each specimen group, splitting tensile tests were conducted on all groups using a WAW-300 universal testing machine. The compressive testing procedure and the specimens after splitting tensile failure are shown in Figure 16.



(**a**) Splitting test (**b**) Specimen after splitting failure

Figure 16. Splitting test of the specimen.

As the number of freeze–thaw cycles increased, the morphology of the splitting surface transitioned from transgranular fracture through aggregates to interfacial failure along the aggregate boundaries. After multiple freeze–thaw cycles, surface spalling was observed, which is considered the primary cause of the sharp decline in splitting tensile strength. Following 100 freeze–thaw cycles, the steel fibers enabled the specimen to maintain a certain level of integrity, reflecting the bridging effect of the fibers.

3.3. Scanning Electron Microscopy (SEM) Analysis After Freeze–Thaw Cycles

The morphology of the microstructure of concrete specimens can, to some extent, influence the macroscopic mechanical properties. The incorporation of steel fibers into concrete materials alters the microstructure of the concrete, which is reflected in its macroscopic physical and mechanical characteristics. By comparing and analyzing the microstructures of steel fiber-reinforced concrete and plain concrete using scanning electron microscopy, this study examines the quantity and morphology of hydration products in the concrete matrix and the interfacial transition zone, as well as the number of cracks and pores, along with the working mechanism of steel fibers, thereby providing explanations for macroscopic test results.

3.3.1. Scanning Electron Microscope Equipment

The microstructural morphology of the specimens was observed using a Zeiss Sigma 300 thermal field-emission scanning electron microscope (FESEM), as illustrated in Figure 17. The analysis primarily aimed to validate the effect of steel fiber addition on improving concrete performance and to investigate the mechanism by which freeze–thaw cycles induce microstructural changes. The FESEM provides a resolution of at least 1.2 nm

at 15 kV (secondary electron image), a magnification range of 10 to 1,000,000×, an adjustable accelerating voltage from 0.02 to 30 kV, and a maximum beam current of at least 20 nA. The instrument accommodates samples in various forms, including dry bulk solids, slices, fibers, and powders.

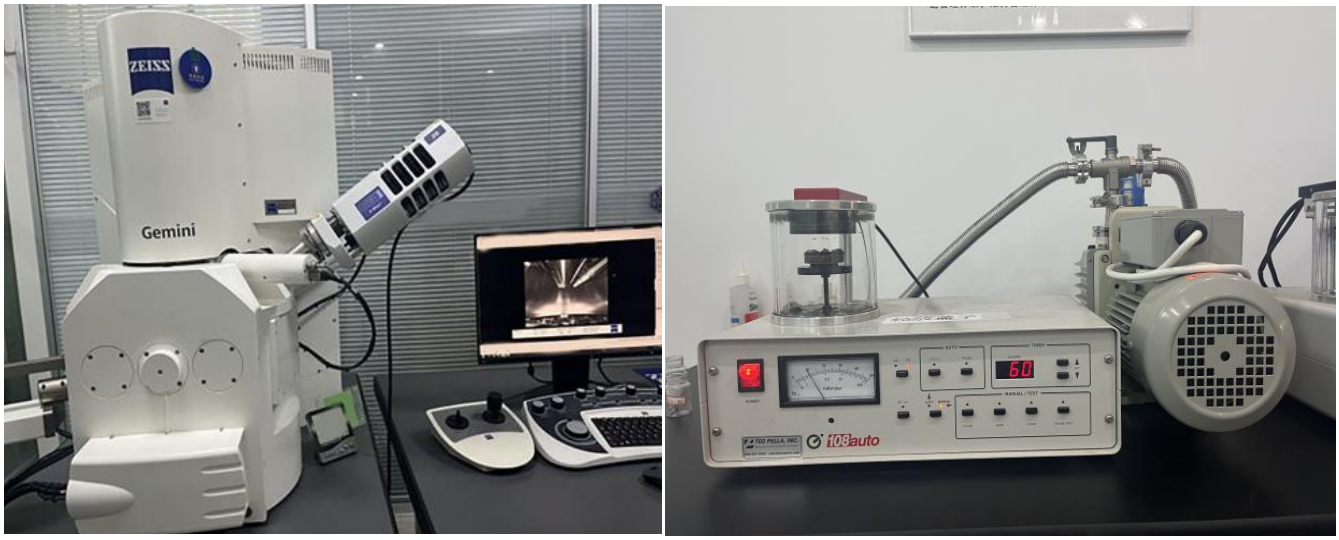

(**a**) Scanning Electron Microscope (**b**) Sample Gold Sputtering Equipment

Figure 17. Microscopic testing equipment.

After processing, small pieces of the concrete specimens were collected and placed in sample bottles for transport to the scanning electron microscopy laboratory. The samples were then cleaned with anhydrous ethanol and dried to a constant weight, as illustrated in Figure 18.



(**a**) Test specimen (**b**) Specimen placement

Figure 18. Specimen preparation for testing.

3.3.2. Analysis of Microscopic Test Results

The comparative scanning electron microscopy (SEM) images of plain concrete and steel fiber-reinforced concrete subjected to 0, 25, 50, 75, and 100 freeze–thaw cycles are presented in Figures 19 and 20, respectively.

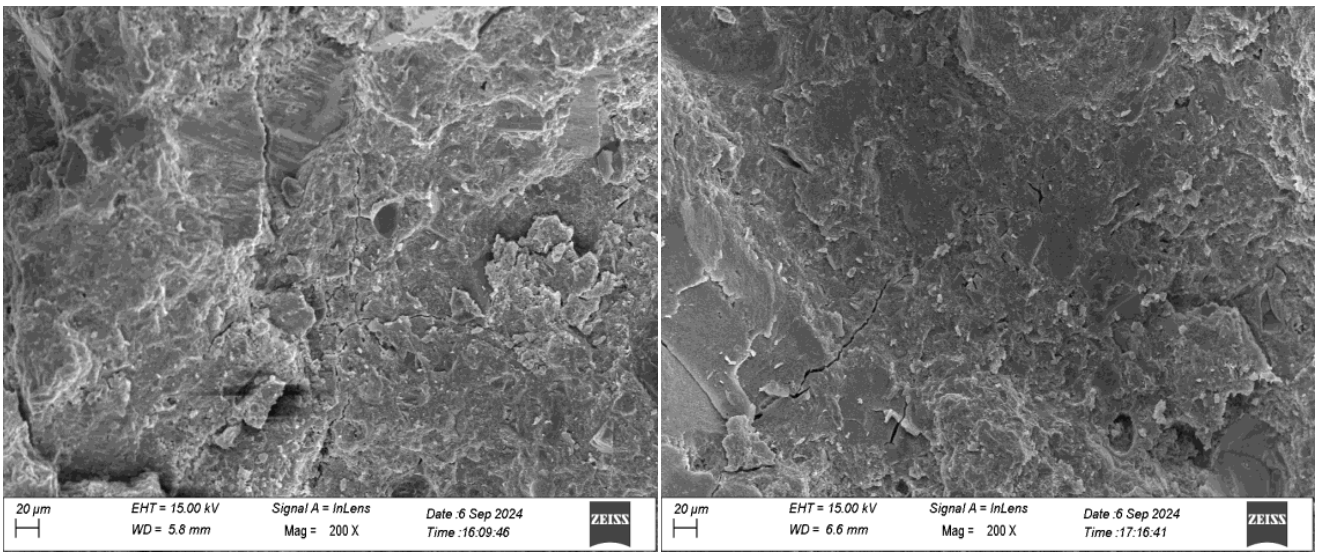

(**a**) S-0 freeze–thaw cycles (0% fiber) (**b**) SF4-0 freeze–thaw cycles (1.5% fiber)

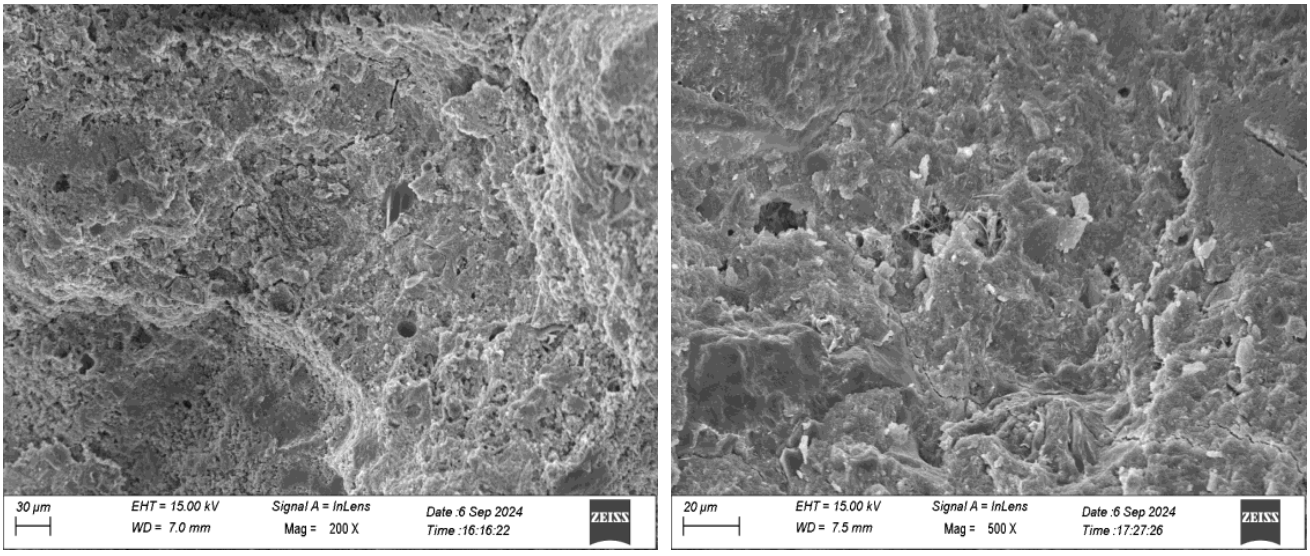

(**c**) S-25 freeze–thaw cycles (0% fiber) (**d**) SF4-25 freeze–thaw cycles (1.5% fiber)

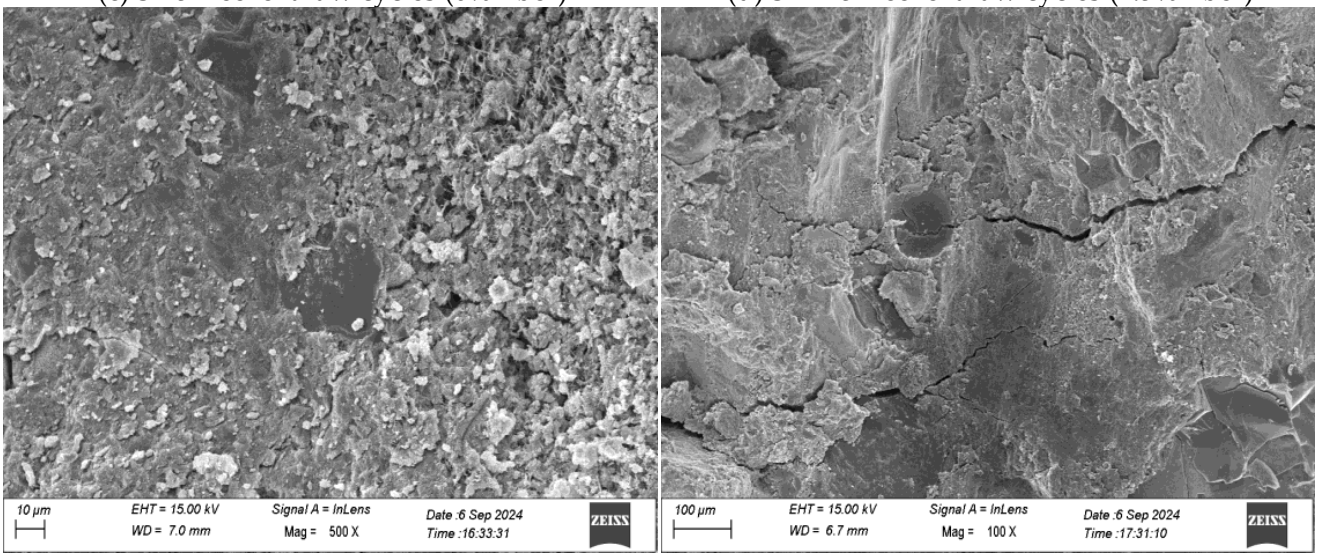

(**e**) S-50 freeze–thaw cycles (0% fiber) (**f**) SF4-50 freeze–thaw cycles (1.5% fiber)

Figure 19. *Cont.*

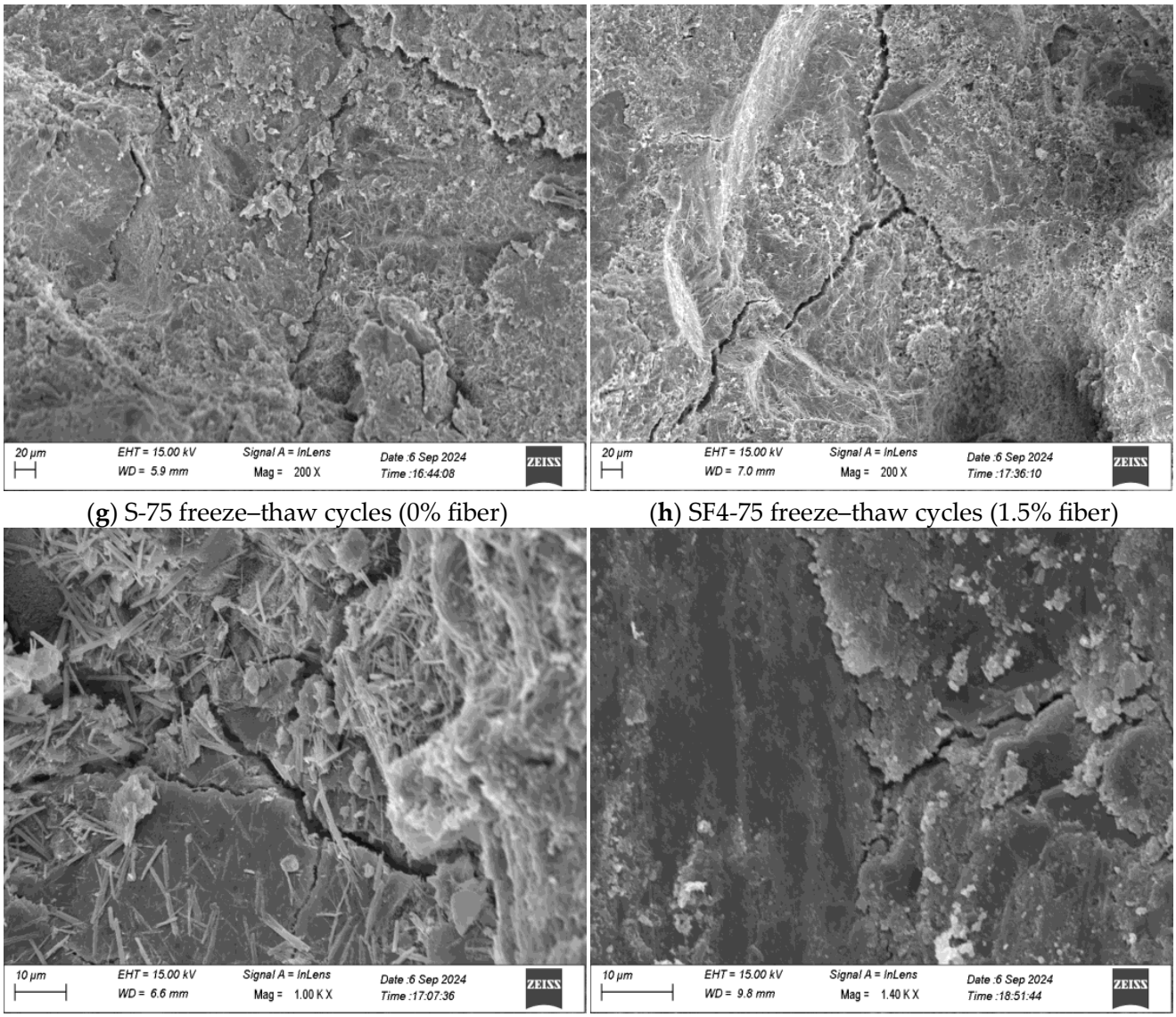

(**g**) S-75 freeze–thaw cycles (0% fiber) (**h**) SF4-75 freeze–thaw cycles (1.5% fiber)

(**i**) S-100 freeze–thaw cycles (0% fiber) (**j**) SF4-100 freeze–thaw cycles (1.5% fiber)

Figure 19. Microstructural morphology of plain concrete and steel fiber-reinforced concrete.

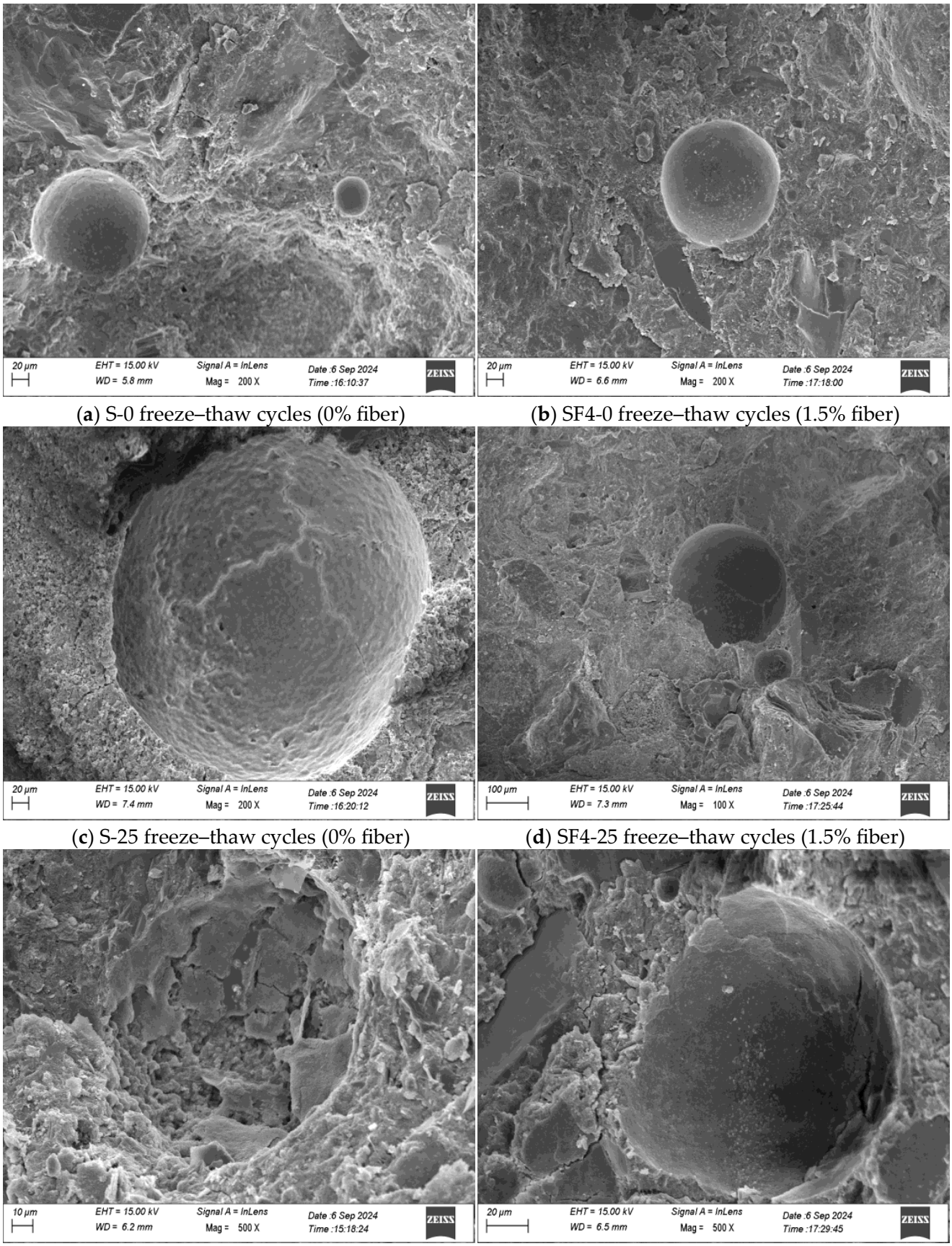

(**a**) S-0 freeze–thaw cycles (0% fiber) (**b**) SF4-0 freeze–thaw cycles (1.5% fiber)

(**c**) S-25 freeze–thaw cycles (0% fiber) (**d**) SF4-25 freeze–thaw cycles (1.5% fiber)

(**e**) S-50 freeze–thaw cycles (0% fiber) (**f**) SF4-50 freeze–thaw cycles (1.5% fiber)

Figure 20. *Cont.*

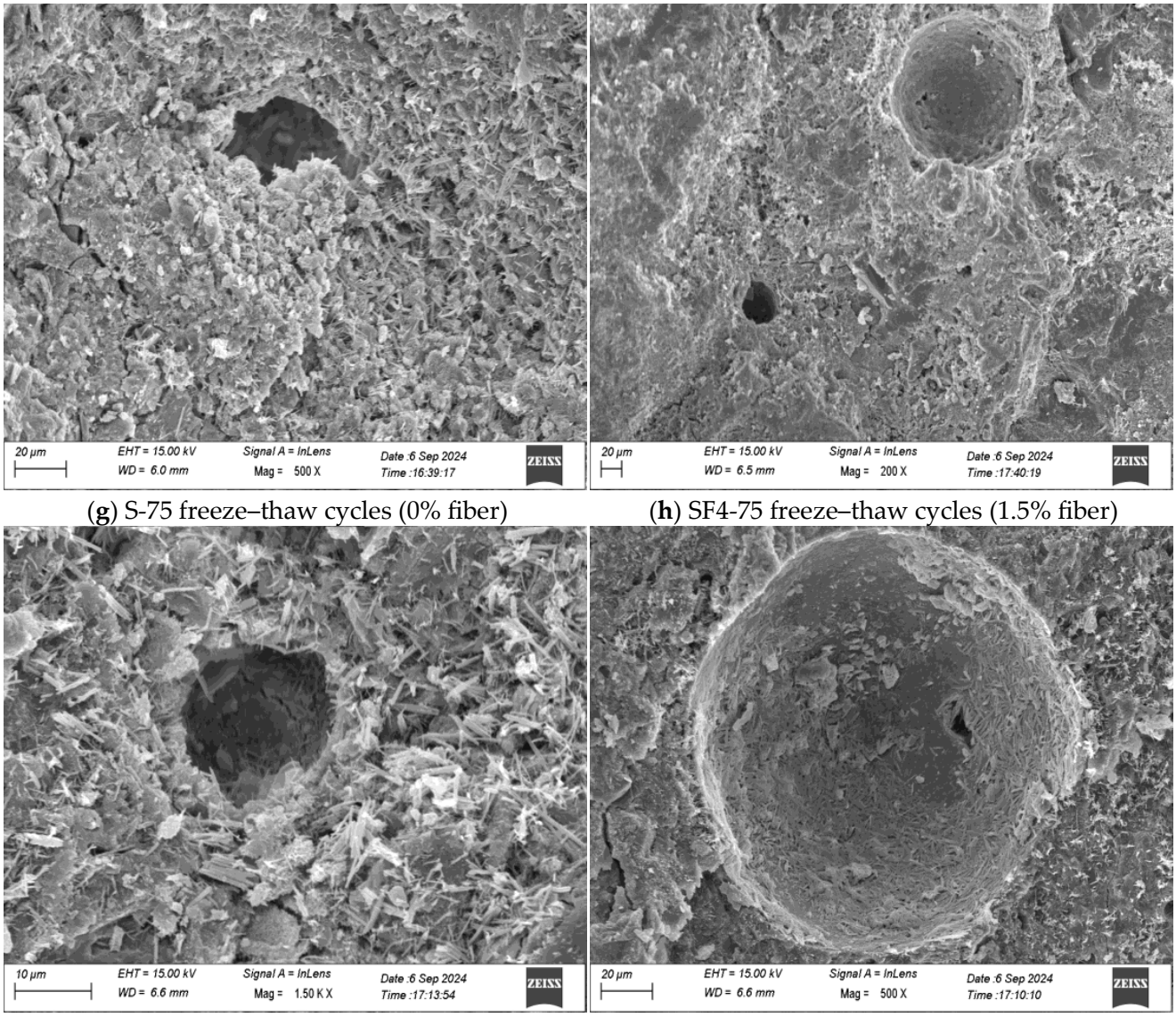

(**g**) S-75 freeze–thaw cycles (0% fiber) (**h**) SF4-75 freeze–thaw cycles (1.5% fiber)

(**i**) S-100 freeze–thaw cycles (0% fiber) (**j**) SF4-100 freeze–thaw cycles (1.5% fiber)

Figure 20. Evolution of pore damage in plain concrete and steel fiber-reinforced concrete.

As can be seen from Figure 19, before freeze–thaw cycles, both plain concrete and steel fiber-reinforced concrete exhibited good structural integrity, high density, and few micro-cracks. With an increase in the number of freeze–thaw cycles, the repeated freezing, expansion, contraction, and seepage pressure of moisture inside the concrete gradually increased, expanded, and interconnected the micro-cracks, resulting in a loosened structure. Notably, the development of cracks and the rate of structural deterioration in plain concrete were significantly faster than those in steel fiber-reinforced concrete. This explains why the five indicators of the macro-specimen decreased with the increase in freeze–thaw cycles.

Microscopic experiments indicate that, under the same number of freeze–thaw cycles, steel fiber-reinforced concrete exhibits fewer internal pores and better structural integrity compared to plain concrete. The primary reasons include the water-retention effect of steel fibers, which promotes more complete hydration reactions in the concrete, resulting in the formation of denser and more uniform hydration products. Furthermore, the interwoven distribution of steel fibers acts similarly to a reinforcement mesh, dispersing stress concentrations at crack tips and effectively inhibiting the propagation rate and extent of cracks.

Based on the results of the microscopic specimens shown in Figure 20, the following observations can be made: ① Before freeze–thaw cycles (a, b), both plain concrete and steel fiber-reinforced concrete exhibited intact pore structures with smooth pore walls and no visible micro-cracks, which is consistent with their macro-morphology and mechanical performance results. After 25 freeze–thaw cycles, a few short and narrow micro-cracks appeared on the pore walls of plain concrete, while the pore walls remained relatively smooth, resulting in minimal impact on the mechanical properties of steel fiber-reinforced concrete. ② After 50 freeze–thaw cycles (e, f), the pore walls of plain concrete were largely disintegrated, with cracks penetrating the loose matrix, exhibiting flaky and craze-like patterns, indicating severe freeze–thaw damage and significant strength loss. In steel fiber-reinforced concrete, the number of micro-cracks increased, and longer cracks appeared on the pore walls, but the overall integrity remained relatively good. ③ After 75 freeze–thaw cycles (g, h), the pore walls of plain concrete collapsed, and the matrix became loose, indicating severe damage and a substantial increase in strength loss across all metrics. For steel fiber-reinforced concrete, the number of micro-cracks further increased, pore walls became rougher with more micro-cracks, and the density of the matrix decreased, leading to a notable acceleration in strength deterioration. ④ After 100 freeze–thaw cycles (i, j), the pore walls of plain concrete completely collapsed, and the matrix became highly fragmented, indicating extremely severe damage with a sharp increase in mass loss, strength loss, and elastic modulus loss. In steel fiber-reinforced concrete, the pore walls became rough, cracks formed a networked structure, the matrix loosened, and the damage became severe, resulting in a significant increase in the loss of all performance indicators.

In summary, the incorporation of silica fume during freeze–thaw cycles can, to some extent, reduce the loss in elastic modulus and strength, validating its enhancing effect on frost resistance. The analysis of concrete's internal structural morphology and damage conditions through microscopic experiments provides a robust explanation for the macroscopic test results.

4. Test Results and Analysis

4.1. Compressive Strength Loss

According to the "Standard for Design of Steel Fiber Reinforced Concrete Structures JGJ/T465-2019" [23], the characteristic and design values of compressive strength for steel fiber-reinforced concrete can be determined based on concrete of the same strength grade, and they shall comply with the relevant provisions of the current national standard "Code for Design of Concrete Structures GB 50010-2010, 2024 Edition" [22]. The formula for calculating the compressive strength loss rate is given by Equation (1).

$$f_n = [\frac{f_{cu,0} - f_{cu,n}}{f_{cu,0}}] \times 100\% \quad (1)$$

where f_n is the loss rate of compressive strength of concrete specimens after n freeze–thaw cycles, (%);

$f_{cu,n}$ is the compressive strength of concrete specimens after n freeze–thaw cycles, (MPa);

$f_{cu,0}$ is the initial compressive strength of concrete before n freeze–thaw cycles, (MPa).

The variation curve of cubic compressive strength with the number of freeze–thaw cycles is shown in Figure 21. The compressive strength loss rate of the concrete specimens, calculated using Formula (1), is presented in Figure 22. From the curves, it can be observed that the cubic compressive strength loss rates of specimens S, SF1, SF2, SF3, and SF4 increase with the increasing number of freeze–thaw cycles. When the number of freeze–thaw cycles does not exceed 75, the order of strength loss rates is S > SF4 > SF1 > SF2 > SF3. When the number of freeze–thaw cycles reaches 100, the order becomes S > SF1 > SF3 > SF4 > SF2, with the corresponding compressive strength loss rates being S = 32.62%, SF1 = 30.35%,

SF2 = 19.04%, SF3 = 26.83%, and SF4 = 24.07%. When the steel fiber volume fraction is the same (i.e., for SF1 and SF2, SF3 and SF4), appropriately increasing the silica fume content can effectively reduce the compressive strength loss of the specimens, showing a certain mitigating effect on the cubic compressive strength loss of concrete. After 100 freeze–thaw cycles, the cubic compressive strength loss rate of the plain concrete specimen (S) reached as high as 32.62%.

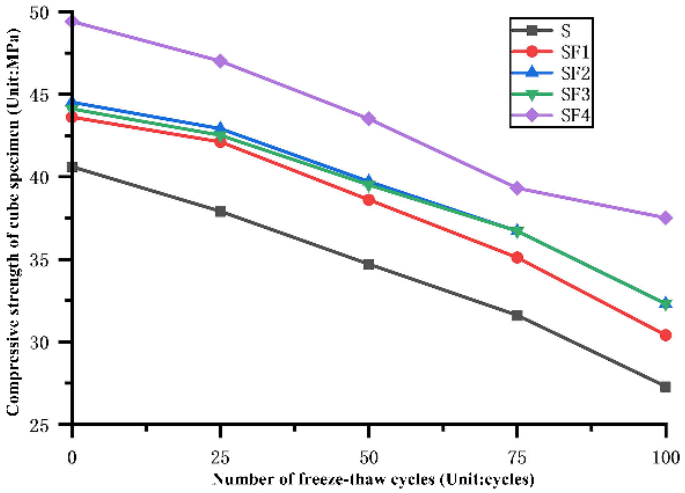

Figure 21. Variation curve of cube compressive strength.

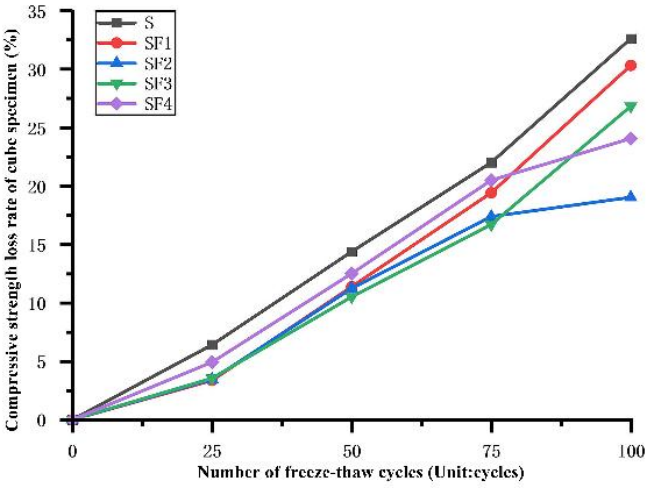

Figure 22. Variation curve of cube compressive strength loss rate.

4.2. Mass Loss

After 25, 50, 75, and 100 freeze–thaw cycles, concrete specimens experience phenomena such as cracking, spalling, and partial detachment due to freeze–thaw action, resulting in changes in specimen mass throughout the cycles. The mass loss rate W_n was adopted as the evaluation index for assessing the mass variation of the freeze–thaw test specimens, calculated using Equation (2) [24].

$$W_n = \frac{G_0 - G_n}{G_0} \times 100\% \quad (2)$$

where W_n is the mass loss rate of concrete specimens after n freeze–thaw cycles, (%);

G_0 is the initial mass of the concrete specimen before the freeze–thaw cycle test, (g);

G_n is the mass of the concrete specimen after n freeze–thaw cycle tests, (g).

The variation curves of mass for each group of specimens versus the number of freeze–thaw cycles are shown in Figure 23. The variation curve of mass loss rate, calculated according to Equation (2), is presented in Figure 24.

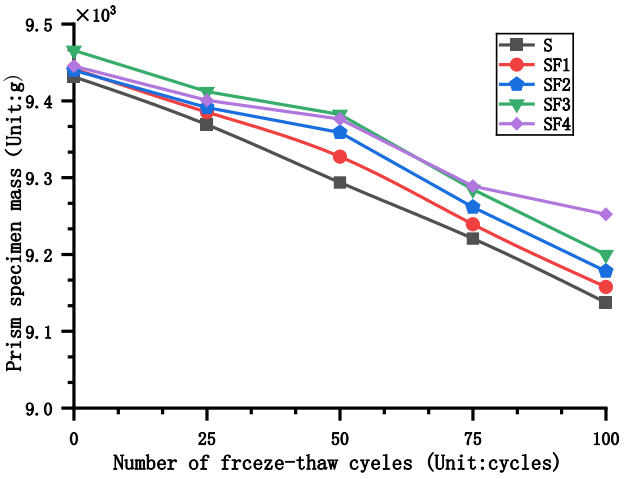

Figure 23. Variation curve of prism specimen mass with the number of freeze–thaw cycles.

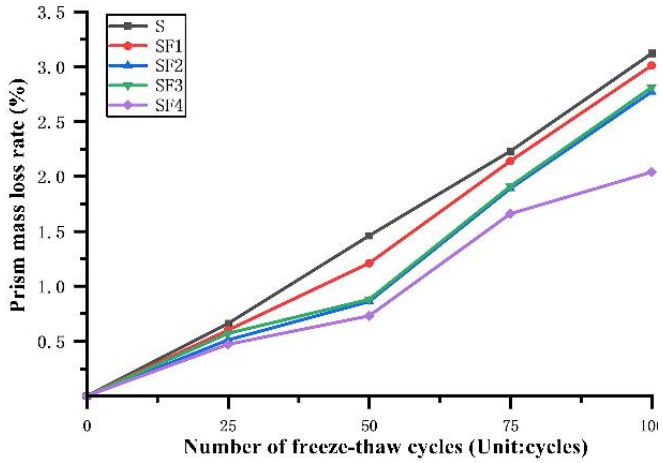

Figure 24. Curve of prism specimen mass change rate versus number of freeze–thaw cycles.

As can be seen, the mass loss rates of specimens S, SF1, SF2, SF3, and SF4 increase with the number of freeze–thaw cycles. At each given cycle count, the mass loss rates follow the order: S > SF1 > SF3 > SF2 > SF4. After 100 freeze–thaw cycles, the mass loss rates for each group are S = 3.12%, SF1 = 3.01%, SF2 = 2.77%, SF3 = 2.81%, and SF4 = 2.04%. When the steel fiber volume fraction is the same (i.e., comparing SF1 with SF2, and SF3 with SF4), appropriately increasing the silica fume content can reduce the specimen's mass loss. Conversely, when the silica fume content is the same (i.e., comparing SF1 with SF3, and SF2 with SF4), appropriately increasing the steel fiber volume fraction also helps lower the mass loss. The results indicate that the incorporation of both steel fibers and silica fume contributes to reducing the mass loss of concrete specimens to some extent. After 100 freeze–thaw cycles, the mass loss rate of plain concrete reached 3.12%.

4.3. Relative Dynamic Elastic Modulus Loss

According to the China Engineering Construction Standardization Association. CECS 13:89 Test methods for steel fiber-reinforced concrete [25], the formula for calculating the flexural strength loss rate of specimens is given as Equation (3):

$$E_{fc,n} = \frac{E_n - E_0}{E_0} \times 100\% \quad (3)$$

where $E_{fc,n}$ is the loss rate of elastic modulus of concrete specimens after n freeze–thaw cycles, (%);

E_n is the elastic modulus of concrete specimens after n freeze–thaw cycles, (MPa);

E_0 is the initial elastic modulus of concrete specimens before n freeze–thaw cycles, (MPa).

The relative dynamic elastic modulus of the prismatic specimens before and after freeze–thaw cycles was measured using a dynamic elasticity modulus tester. The variation in dynamic elastic modulus can reflect the internal damage of concrete, and the specific calculation formula is given as Equation (4) [20].

$$\xi_{fc,n} = \frac{f_{fc,n}^2}{f_{fc,0}^2} \times 100\% \quad (4)$$

where $\xi_{fc,n}$ is the relative elastic modulus value of the concrete specimen after n freeze–thaw cycles, (%);

$f_{fc,n}$ is the transverse fundamental frequency of the concrete specimen after n freeze–thaw cycles, (HZ);

$f_{fc,0}$ is the initial transverse fundamental frequency of the concrete specimen before freeze–thaw cycles, (HZ).

The variation curves of the elastic modulus loss rate and the relative dynamic elastic modulus percentage for each group of specimens are shown in Figures 25 and 26, respectively.

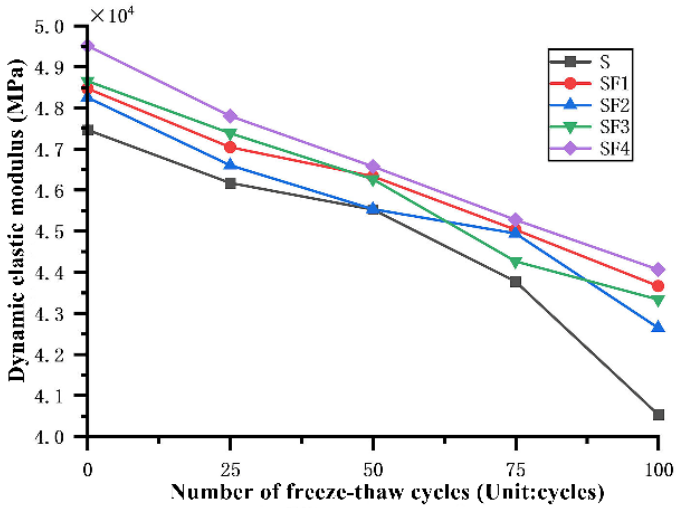

Figure 25. Curve of dynamic elastic modulus of the specimen.

Figure 25 shows the relationship curves between the dynamic elastic modulus loss rate of specimens in each group and the number of freeze–thaw cycles. As can be observed from the curves, the elastic modulus loss rates of the S, SF1, SF2, SF3, and SF4 specimens increase with the rising number of freeze–thaw cycles. It can be seen from Figure 26 that when the specimens undergo 100 freeze–thaw cycles, the relative dynamic elastic modulus loss rates follow the order: S > SF2 > SF4 > SF3 > SF1. The elastic modulus loss rates for each group

are S = 14.60%, SF1 = 9.92%, SF2 = 11.63%, SF3 = 10.94%, and SF4 = 11.01%. When the steel fiber volume ratio is the same (i.e., SF1 and SF2, SF3 and SF4), the incorporation of silica fume leads to a certain increase in the loss of splitting tensile strength of the specimens. The analysis results indicate that with an appropriate silica fume content of 10%, a suitable addition of steel fibers can somewhat reduce the elastic modulus loss rate of concrete specimens. After 100 freeze–thaw cycles, the elastic modulus loss rate of plain concrete specimens reaches as high as 14.60%.

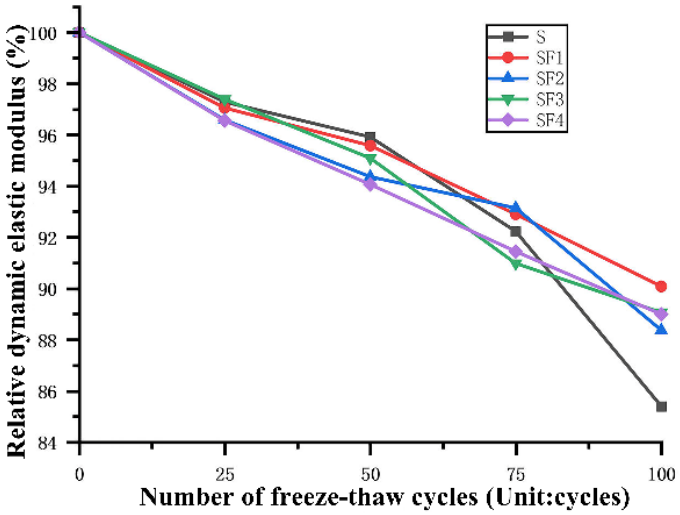

Figure 26. Curve of the relative dynamic elastic modulus of the specimen.

5. Optimum Mix Proportion

From Table 9, it can be observed that the loss rates of mass, compressive strength, flexural strength, splitting tensile strength, and dynamic elastic modulus of the specimens under freeze–thaw cycles are presented. Among these, SF4 exhibits the smallest loss rate in two indicators, SF2 in two indicators, and SF1 in one indicator. The indicator for which SF1 shows the smallest loss rate is splitting tensile strength, which is 7.42% lower than that of SF2 and only 1.17% lower than that of SF4. The reduction in splitting tensile strength for SF4 is minimal, and its strength remains significantly higher than that of SF2. The indicators for which SF2 shows a lower loss rate than SF4 are compressive strength and dynamic elastic modulus. Specifically, the difference in the loss rate of elastic modulus is only 0.63%, suggesting that their loss rates are approximately equivalent. However, the elastic modulus of SF4 is substantially higher than that of SF2. Although the difference in compressive strength loss rate between SF4 and SF2 is 5.03%, the actual compressive strength value of SF4 is much higher than that of SF2.

Table 9. Loss rates of various indicators after 100 freeze–thaw cycles.

Loss Rate	S	SF1	SF2	SF3	SF4	Specimen Number with Minimum Loss
Mass	3.12%	3.01%	2.77%	2.81%	2.04%	SF4
Compressive strength	32.62%	30.35%	19.04%	26.83%	24.07%	SF2
Flexural strength	26.43%	20.03%	16.29%	14.13%	14.08%	SF4
Splitting strength	40.60%	26.70%	34.12%	31.75%	27.87%	SF1
Dynamic modulus of elasticity	14.60%	9.92%	11.63%	10.94%	11.01%	SF2

Therefore, taking into account the physical and mechanical results of the five specimens, it is preliminarily concluded that the material combination of SF4 is optimal. The response surface analysis predicts that SFRC constitutes the optimal combination, as illustrated in Figure 27.

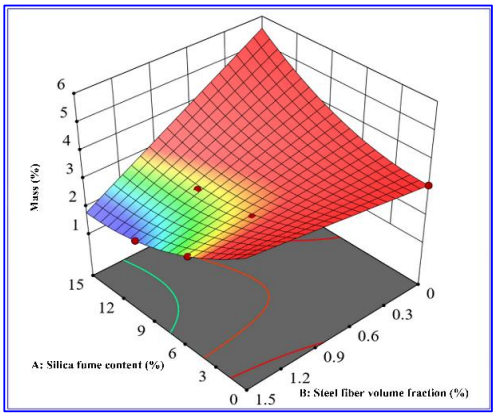

(**a**) Response surface of mass loss

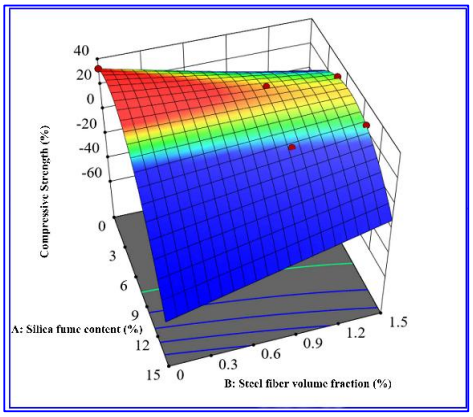

(**b**) Response surface of compressive strength

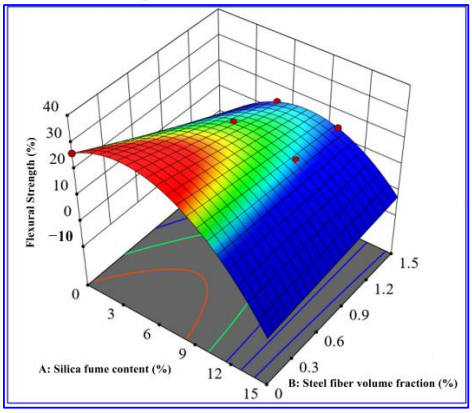

(**c**) Response surface of flexural strength loss

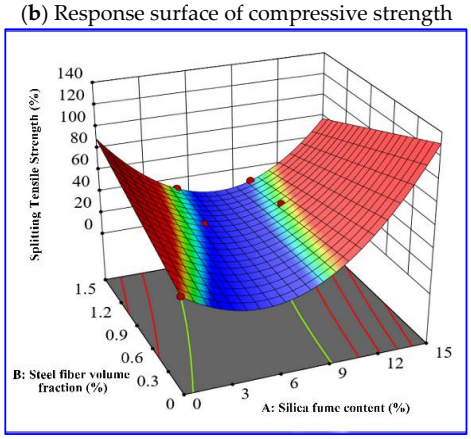

(**d**) Response surface of splitting tensile strength

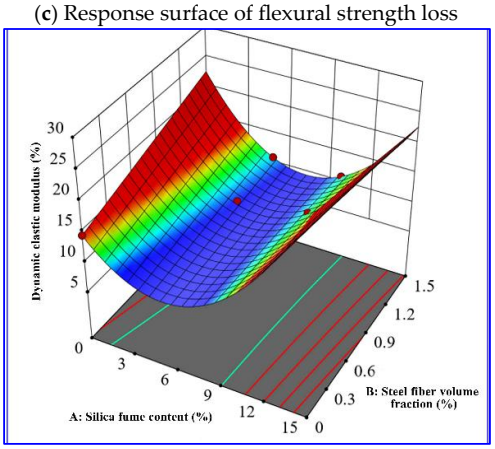

(**e**) Response surface of dynamic elastic modulus loss

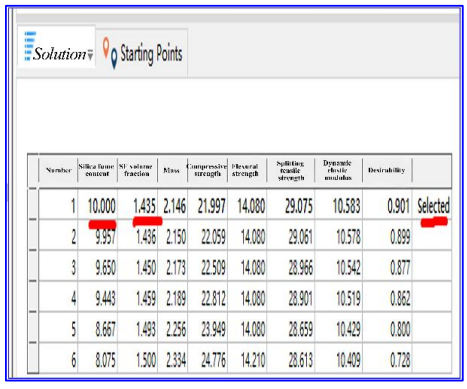

(**f**) Prediction results of response surface analysis

Figure 27. Response surface analysis.

6. Conclusions and Recommendations

This study focuses on steel fiber-reinforced concrete (SFRC), investigating the evolution patterns of its mechanical properties under freeze–thaw conditions through raw material optimization, mix proportion design, specimen preparation, freeze–thaw cycle testing, macro-performance evaluation, and microscopic mechanism analysis. The conclusions are as follows:

(1) Based on the characteristics of cold-region environments, the materials for preparing SFRC were systematically selected. The cementitious materials comprised PO42.5 cement and silica fume with an average particle size of less than 10 μm, while the aggre-

gates included coarse aggregates with a size of 5–10 mm and manufactured sand with a fineness modulus of approximately 2.5. Considering the mechanical and workability performance of SFRC, the silica fume content and steel fiber volume fraction were selected as the core variables. With a fixed water–binder ratio of 0.4 and a water-reducing agent dosage of 1%, five mix proportions were designed to optimize the material combination.

(2) Based on relevant research [5–7] and freeze–thaw test standards, cementitious materials, aggregates, reinforcement phases, and admixtures were selected to formulate a compatible material combination and verify its potential for resisting deterioration, thereby providing a foundation for the experiments. Using an orthogonal experimental design, specimens were fabricated with silica fume content and steel fiber volume fraction as the core variables. Following standard testing protocols, rapid freeze–thaw tests were conducted to ensure experimental stability and data reliability.

(3) Concrete damage due to freeze–thaw cycles intensifies with the number of cycles, with the extent of deterioration ranking as follows: splitting tensile strength, compressive strength, flexural strength, dynamic elastic modulus, and mass. Steel fibers can significantly mitigate this damage. When the fiber content is fixed, increasing the silica fume dosage reduces the mass loss as well as the losses in compressive and flexural strengths, but it increases the loss in dynamic elastic modulus. The loss in splitting tensile strength increases at a fiber content of 1% but decreases at 1.5%. When the silica fume dosage is fixed, increasing the fiber content reduces mass loss and flexural strength loss, while the change in dynamic elastic modulus is minimal. The compressive strength loss decreases at a silica fume dosage of 5% but increases at 10%. The trends in splitting tensile strength and dynamic elastic modulus show opposite patterns under these conditions.

(4) Based on a comprehensive analysis of the loss rates of various indicators after 100 freeze–thaw cycles, the performance ranking of the material combinations from optimal to weakest is as follows: SF4 > SF2 > SF3 > SF1 > S. Consequently, SF4 is selected as the optimal mix proportion. Microscopic scanning electron microscopy (SEM) reveals the internal structural morphology and damage characteristics, providing a reasonable explanation for the results of the macroscopic performance tests. This study provides reference directions for further enhancing the frost resistance of SFRC. Future research can explore strategies such as the incorporation of stone powder and the application of a higher silica fume content (15–20%), and validate the long-term durability under coupled freeze–thaw and erosion environments.

Author Contributions: The authors confirm contribution to the paper as follows: Conceptualization, L.-M.W.; methodology, F.G.; software, Y.W.; validation, F.G. and L.-M.W.; formal analysis, F.G.; investigation, Z.-J.W.; data curation, H.-X.-T.H.; writing—original draft preparation, L.-M.W.; writing—review and editing, Y.W. and H.-X.-T.H.; visualization, H.-X.-T.H. and W.-J.L.; supervision, G.-N.L.; project administration, L.-M.W.; funding acquisition, L.-M.W. All authors have read and agreed to the published version of the manuscript.

Funding: This work was supported by the Science and Technology Research Program of Chongqing Municipal Education Commission (Grant No. KJZD-K202504002; No. KJQN202304008; No. KJZD-K202404003).

Institutional Review Board Statement: (1) The committee that approved the study. (2) The compliance documents.

Data Availability Statement: All data involved in this study are included in this paper.

Conflicts of Interest: The authors declare no conflict of interest.

References

1. Lin, Y.; Jiang, S.; Guo, S.; Sun, L. Experimental Research on the Mechanical Properties of Steel Fiber-Reinforced Concrete Under Freeze-Thaw Cycles. *Ind. Constr.* **2025**, *55*, 73–85. [CrossRef]
2. Sun, S.; Fan, X.; Wang, L.; Wang, S.; Wang, S.; Zhang, S. Experimental study on impact resistance of steel fiber reinforced concrete after freeze-thaw cycles. *China Concr. Cem. Prod.* **2025**, *69*, 59–63. [CrossRef]
3. Ding, X.; Zhou, R.; Wang, Y. Effect of silica fume on the frost resistance and pore structure of concrete. *Concrete* **2017**, *1*, 53–55. [CrossRef]
4. Xuan, D.X.; Shui, Z.H.; Wu, S.P. Influence of silica fume on the interfacial bond between aggregate and matrix in near-surface layer of concrete. *Constr. Build. Mater.* **2009**, *23*, 2631–2635. [CrossRef]
5. Xinxin, Z.; Liang, H.; Wenqi, L.; Pengpeng, Z.; Zhaoning, Z. Experimental research on mechanical properties of silica fume recycled concrete after freeze-thaw cycles. *Concrete* **2024**, *1*, 138–142. [CrossRef]
6. Tao, Z.; Xiaobin, X.; Yan, L. Research on the Influence of freeze-thaw cycles on dynamic performance of steel fiber reinforced concrete. *J. Water Resour. Water Eng.* **2021**, *32*, 167–172, 178. Available online: https://qikan.cqvip.com/Qikan/Article/Detail?id=7105374908 (accessed on 20 January 2026).
7. Min, B.; Ditao, N.; Lei, J.; Miao, Y. Research on Improving the Mechanical Properties and Microstructure of Concrete with Steel Fiber. *Bull. Chin. Ceram. Soc.* **2013**, *32*, 2084–2089. [CrossRef]
8. Fangyuan, D.; Hanpeng, W.; Jiangtao, Y.; Keke, L.; Zhenwen, G.; Xinzhi, D.; Qiong, X. Effect of freeze–thaw cycling on mechanical properties of polyethylene fiber and steel fiber reinforced concrete. *Constr. Build. Mater.* **2021**, *295*, 123427. [CrossRef]
9. Xinyu, Z.; Yingrui, W.; Shaoqi, Z.; Fei, X.; Xinping, Z.; Xi, J.; Long, Z.; Yi, S.; Qing, C.; Zhiguo, Y.; et al. Research progress of the thermophysical and mechanical properties of concrete subjected to freeze-thaw cycles. *Constr. Build. Mater.* **2022**, *330*, 127254. [CrossRef]
10. Yunyan, L.; Hu, C. *Experimental Design and Data Processing*, 3rd ed.; Chemical Industry Press: Beijing, China, 2017.
11. Chenxia, W.; Lu, L.; Fubo, C.; Lan, L. Experimental study on mechanical properties of recycled concrete after freeze-thaw cycles. *J. Build. Struct.* **2020**, *41*, 193–202. [CrossRef]
12. *GB 175-2007*; Common Portland Cement. Standards Press of China: Beijing, China, 2007.
13. Wenqi, L.; Liang, H.; Zhaoning, L.; Xiaowen, F.; Xuepeng, W.; Yao, X.; Zhang, X. Freezing resistance performance and finite element analysis of silica ash recycled concrete. *Concrete* **2025**, *1*, 21–25.
14. *GB/T 27690-2023*; Silica Fume for Mortar and Concrete. China Standards Press: Beijing, China, 2023.
15. *JTG 3432-2024*; Test Methods for Aggregate in Highway Engineering. China Communications Press: Beijing, China, 2024.
16. *GB/T 14684-2022*; Sand for Construction. Standards Press of China: Beijing, China, 2022.
17. *GB 8076-2023*; Concrete Admixtures. Standards Press of China: Beijing, China, 2023.
18. *JT/T 524-2019*; Fibers for Cement Concrete in Highway Engineering. China Communications Press: Beijing, China, 2019.
19. Huibin, S.; Huixiang, Y.; Jianhong, W.; Yunfa, H.; Zhao, C. Experimental study on the influence of different feeding process on the compressive strength of steel fiber reinforced concrete. *J. Shandong Jianzhu Univ.* **2025**, *40*, 7–12. Available online: https://qikan.cqvip.com/Qikan/Article/Detail?id=7202025124 (accessed on 20 January 2026). [CrossRef]
20. *GB/T 50082-2024*; Standard for Test Methods of Long-Term Performance and Durability of Concrete. China Architecture & Building Press: Beijing, China, 2024.
21. *GB/T 39147-2020*; Steel Fibres for Concrete. Standards Press of China: Beijing, China, 2020.
22. *GB 50010-2010*; Code for Design of Concrete Structures. China Architecture & Building Press: Beijing, China, 2024.
23. *JGJ/T 465-2019*; Standard for Design of Steel Fiber Reinforced Concrete Structures. China Architecture & Building Press: Beijing, China, 2019.
24. *GB/T 50081-2019*; Standard for Test Methods of Concrete Physical and Mechanical Properties. China Architecture & Building Press: Beijing, China, 2019.
25. *CECS 13:89*; Test Methods for Steel Fiber Reinforced Concrete. China Engineering Construction Standardization Association: Beijing, China, 1990.

Disclaimer/Publisher's Note: The statements, opinions and data contained in all publications are solely those of the individual author(s) and contributor(s) and not of MDPI and/or the editor(s). MDPI and/or the editor(s) disclaim responsibility for any injury to people or property resulting from any ideas, methods, instructions or products referred to in the content.